J Nanopart Res (2012) 14:984
DOI 10.1007/s11051-012-0984-4

RESEARCH PAPER

Magnetic carbon nanotubes: synthesis by a simple solvothermal process and application in magnetic targeted drug delivery system

Deli Xiao · Pierre Dramou · Hua He · Lien Ai Pham-Huy · Hui Li · Yuyang Yao · Chuong Pham-Huy

Received: 11 January 2012 / Accepted: 8 June 2012 / Published online: 22 June 2012

Abstract In this study, a new synthesis technique of magnetic multiwall carbon nanotubes (MMWCNTs) was achieved and its application for drug-loading ability was assessed. MMWCNTs were prepared by a simple solvothermal process, which can easily alter the size (100–350 nm), location, and denseness of Fe_3O_4 beads fixed on MWCNTs as well as the MWCNTs structure via controlling the reaction parameters. The characteristics of MMWCNTs obtained were assessed by scanning electron microscopy, X-ray diffraction, and FTIR. The MMWCNTs were used as a drug carrier to load an anticancer molecule, epirubicin hydrochloride. In addition, its adsorption ability was also evaluated. The Freundlich adsorption model was successfully used to describe the adsorption process. The kinetic data was well fitted with a pseudo-second-order model. Due to its magnetic properties, high adsorption surfaces, and excellent adsorption capacities, the MMWCNTs synthesized in this study are suitable to be applied to a magnetic targeted drug delivery system.

Keywords Magnetic multiwall carbon nanotubes · Solvothermal process · Epirubicin hydrochloride · Drug delivery · Nanomedicine

Introduction

Carbon nanotubes (CNTs), discovered in 1991 by Iigyma (1991), are now considered to be a top-class subject in academic researches as well as in various industrial areas. They have become one of the most promising candidates for drug delivery system in nanomedicine and pharmaceutical industry, due to their ultra-high surface area, high mechanical strength, excellent chemical and thermal stability, and rich electronic polyaromatic structure. CNTs have been proven to be an excellent carrier for a wide variety of bio-molecules, including drugs (Liu et al. 2007; Yang et al. 2009), peptides (Pantarotto et al. 2004), and proteins (Graff et al. 2008). Many studies have demonstrated that when bonded to CNTs, these molecules are delivered more

Deli Xiao and Pierre Dramou contributed equally to this study and should be considered co-first authors.

D. Xiao · P. Dramou · H. He (✉) · H. Li · Y. Yao
Department of Analytical Chemistry, China Pharmaceutical University, Nanjing 210009, China
e-mail: jcb315@163.com

H. He
Key Laboratory of Drug Quality Control and Pharmacovigilance, Ministry of Education, China Pharmaceutical University, Nanjing 210009, China

L. A. Pham-Huy
Department of Pharmacy, Stanford University Medical Center, Palo Alto, CA, USA

C. Pham-Huy
Faculty of Pharmacy, University of Paris V, 4 Avenue de l'Observatoire, 75006 Paris, France

effectively and safely into cells than by traditional methods (Pavani and Vinay 2011). Recently, several disadvantages of CNTs, such as poor dispersity in aqueous media, metabolic pathway and toxicity, have caused extensive concern. Covalent (Hong et al. 2005) or non-covalent (Bottini et al. 2006) modification methods have been introduced to stabilize the dispersity of CNTs in aqueous media. The potential applications in vivo are intensely related to the metabolic pathway of CNTs in animals. Wang et al. (2004) have reported that modified CNTs were mainly metabolized through the urine with little liver intake. Moreover, by comparison with pristine CNTs (Dumortier et al. 2006), many researchers have discovered that functionalized CNTs display very low toxicity in vivo. These results lay a foundation for further study of CNTs in therapeutic applications.

Magnetite nanocrystals have been widely studied because of their potential applications in nanomedicine such as biological labeling, magnetic resonance imaging, and targeted drug delivery (Sun et al. 2000; Nam et al. 2003; Gao et al. 2007; Cai et al. 2009; Gai et al. 2010). In recent years, more and more researchers have a tendency to combine CNTs with iron oxide for MMWCNTs preparation. Various MMWCNTs synthesis methods have been described in the literature. Correa-Duarte et al. (2005) have synthesized MMWCNTs through a layer-by-layer assembly approach. Georgakilas et al. (2005), have used pyrene as interlinker for the attachment of capped magnetic nanoparticles (MNPs) on the CNTs surface. Gao et al. (2006), have prepared MMWCNTs via the electrostatic attraction between CNTs and MNPs. Jia et al. (2007), have combined magnetite beads with CNTs based on a hydrothermal technique. According to these reports, there are two different modes to combine the magnetic materials with the CNTs: (1) encapsulating MNPs in CNTs or (2) attaching MNPs on the surface of CNTs. Even though there have been a number of reports about successful synthesis of MMWCNTs (Gao et al. 2006; Jia et al. 2007; Kim et al. 2010; Zhu et al. 2010; Korobeinyk et al. 2011), the size, denseness, and location of Fe_3O_4 beads along MWCNTs as well as the structure of Fe_3O_4/MWCNTs composite remain unresolved problems. These problems are important for Fe_3O_4/MWCNTs composite to penetrate into the cells to promote the cellular uptake of therapeutic molecules, but unfortunately, only a few reports involve this kind of study so far (Jia et al. 2007).

Epirubicin hydrochloride (EPI) is an effective anthracycline cytostatic antibiotic with a wide antineoplastic spectrum. However, it can lead to severe depressing of hematopoiesis and cardiac toxicity. Prevalent researches have illustrated that the foremost method to minimize the side effects of EPI is to explore a new drug carrier which can change the biological distribution of EPI and target the local tumor. Nowadays, several researches have proved that CNTs can be the carrier of drugs, peptides, and nucleic acids by forming stable covalent or non-covalent bonds. Also, its capacity to permeate into the cells to increase the cellular uptake of therapeutic molecules has been proved (Bianco et al. 2005). These discoveries have provided new opportunities in nanomedicine and nanobiotechnology. The efficacy of most of the existing drugs which have small molecules is restricted not only by their systemic toxicity and narrow therapeutic window, but also due to the drug resistance and limited cellular penetration. According to the above reasons, it is necessary to enhance cellular uptake of EPI by developing efficient and targeted drug delivery systems.

In this study, a simple solution to these problems was demonstrated using novel MMWCNTs nanostructures with new synthesis technique, in which the location, size, and denseness of MNPs on CNTs were easy to control. Furthermore, we systematically investigated the adsorption behavior and mechanism of EPI on MMWCNTs. Although several studies have investigated drug-CNTs complex, the adsorption behavior of EPI on MMWCNTs has never been reported in literature. The results of this study were expected to provide a theoretical basis and offer new methods for preparation of efficient magnetic targeted drug delivery systems.

Experimental

Materials 试剂

Ferric chloride hexahydrate ($FeCl_3 \cdot 6H_2O$), sodium acrylate (CH_2=CHCOONa, Na acrylate), sodium acetate (CH_3COONa, NaOAc), ethylene glycol (EG), and diethylene glycol (DEG) were obtained from Aladdin. EPI was from Shandong New Time

Pharmaceutical Co., Ltd., China. Carbon nanotubes with outer diameter 10–20 nm and length 5–15 μm were purchased from Shenzhen Nanotechnologies Port Co., Ltd., China.

Carboxylation of MWCNTs

Carboxylation of MWCNTs (c-MWCNTs) was carried out by adding pristine MWCNTs (0.5 g) with 100 mL of sulfuric acid and nitric acid mixture (mole ratio: 3/1). This solution was dispersed by ultrasonication for about 2 h and refluxed under magnetic stirring at 80 °C for 12 h. Then, the dispersed solution was filtered and the particles obtained were washed to neutrality, and dried in vacuum at 65 °C overnight.

Synthesis of MMWCNTs

In a typical procedure, the preparation of MMWCNTs was carried out by adding c-MWCNTs (0.4 g), $FeCl_3 \cdot 6H_2O$ (2.4 g, 9 mmol), Na acrylate (3.4 g), and NaOAc (3.4 g) into a mixture of EG (33.75 mL) and DEG (11.25 mL) under ultrasonication for about 1 h. The homogeneous black solution obtained was transferred to a Teflon-lined stainless-steel autoclave and sealed to heat at 200 °C. After reaction for 10 h, the autoclave was cooled to room temperature. The MMWCNTs obtained were washed several times with ethanol and water, and then dried in vacuum at 65 °C for 10 h. In parallel, a reference was prepared by the same protocol with MNPs, but without adding c-MWCNTs.

Characterization 仪器

The size and morphology of the synthesized MMW CNTs were characterized by S-3000 scanning electron microscopy (SEM, Hitachi Corporation, Japan) and a FEI Tecnai G2 F20 transmission electron microscope (TEM). Phase identification was done by the X-ray powder diffraction pattern (XRD), using X′ TRA X-ray diffractometer with Cu Kα irradiation at $\gamma = 0.1541$ nm. The surface groups on MMWCNTs were measured with a 8,400 s FTIR spectrometer (Shimadzu Corporation, Japan).

Adsorption experiments 2.3.3

For kinetic study, 50 mL of 300 μg/mL EPI aqueous solution (pH 7.0) were agitated with 0.05 g c-MWCNTs, MNPs, MMWCNTs, respectively. Samples were taken at different time intervals until the adsorption reached equilibrium.

Static equilibrium adsorption experiments were conducted using screw-capped glass centrifuge tubes as batch reactor systems. Each tube containing 0.01 g c-MWCNTs, MNPs, MMWCNTs, respectively were filled with 10 mL EPI aqueous solution at different concentrations. All tubes were immediately sealed and shaken with a rotary shaker at 150 rpm for 4 h.

All experiment batches were carried out at ambient temperature (25 ± 2 °C). c-MWCNTs were separated from the mixture by centrifugation (13,000 rpm for 1 h), while MNPs and MMWCNTs were isolated from the mixture with a magnet. The amount of EPI adsorbed was calculated by the difference between the initial and residual EPI amounts found in solution divided by the weight of the c-MWCNTs, MNPs, MMWCNTs, respectively.

In vitro release of EPI 2.3.4

For the drug release study, the suspensions of the EPI-loaded MMWCNTs (20 mg) were allowed to stand at 37 °C in phosphate-buffered saline (PBS) solutions (50 mL) at different pH values. The released medium (1 mL) was withdrawn at predetermined time intervals and replaced with equal volumes of fresh medium. The released amount of EPI was determined by UV–Vis spectrophotometry.

Results and discussion

Characterization of c-MWCNTs, MNPs, and MMWCNTs 磁性纳米粒子

The morphologies of pristine MWCNTs, c-MWCNTs, MNPs, and MMWCNTs were obtained by SEM and TEM (Fig. 1). It was observed that the length of c-MWCNTs seemed to be shorter than that of pristine MWCNTs (Fig. 1a, b). All of the pristine MWCNTs were curled and entangled (Fig. 1a). With oxidation, the c-MWCNTs were seen with more open ends (bright spots on the image) with granular surface and joining tubes together (Fig. 1b). Some bundles appeared exfoliated and showed more open ends. The SEM results also indicated that the c-MWCNTs became reactive at the ends as well as at the sidewalls

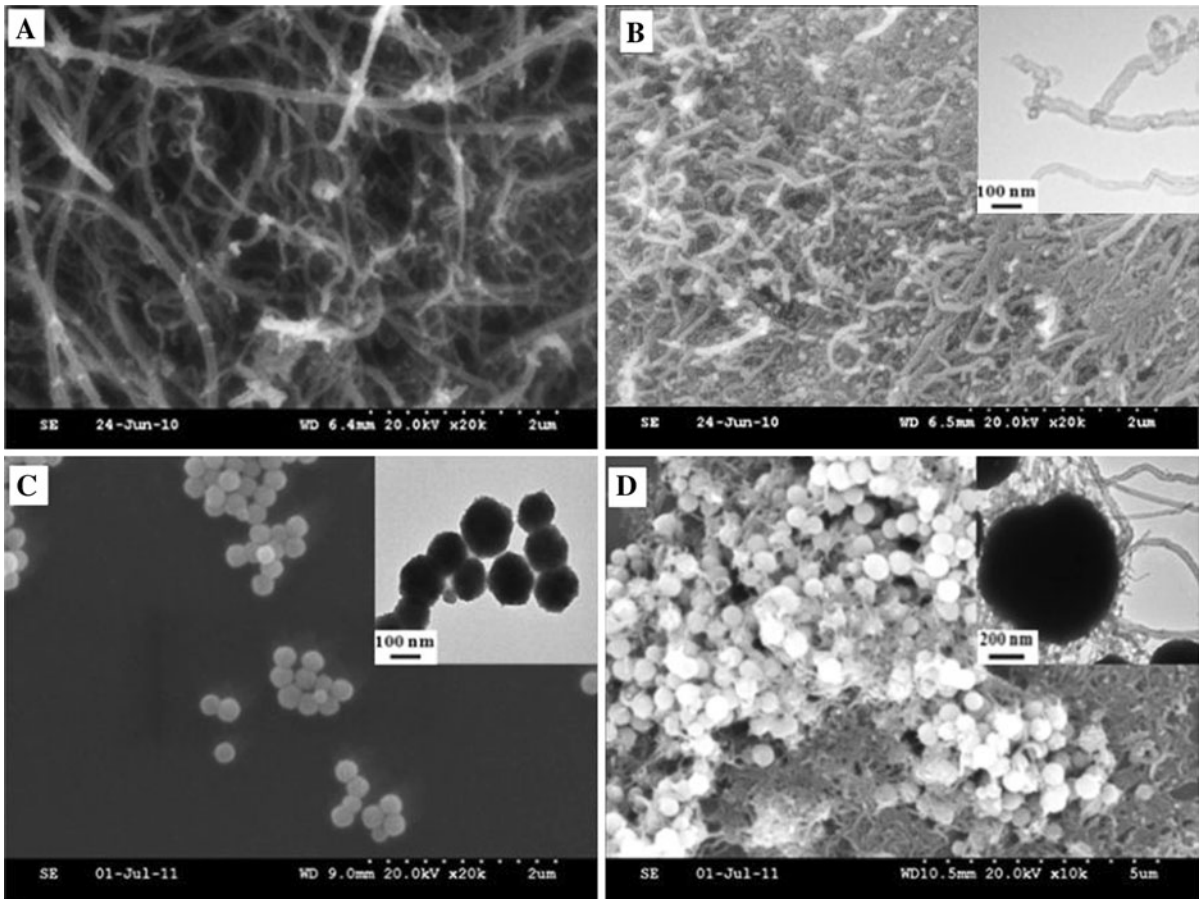

Fig. 1 SEM and TEM images of **a** MWCNTs, **b** c-MWCNTs (*inset* TEM of c-MWCNTs), **c** MNPs (*inset* TEM of MNPs), and **d** MMWCNTs (*inset* TEM of MMWCNTs)

(Kim et al. 2006). MNPs were spherical and remarkably uniform with an average size about 170 nm (Fig. 1c). Iron oxide nanoparticles were successfully coated on the surface of MWCNTs to form MMWCNTs (Fig. 1d).

The magnetism and adsorption characteristics of c-MWCNTs, MNPs, and MMWCNTs are displayed in Fig. 2. It was observed that, after dispersion of three kinds of magnetic materials in EPI aqueous solution, the color of the solution changed from red to black, but after shaking the mixture for 60 min only MMWCNTs could be easily separated from the aqueous solution within few seconds by placing a permanent magnet near the glass bottle and the supernatant was colorless (Fig. 2c). This experiment proved that only MMWCNTs possessed both the properties of adsorption capacity and of magnetism.

Figure 3 represents the XRD pattern of the MNPs and MMWCNTs. Compared with MNPs, the XRD pattern of MMWCNTs had the diffraction peaks of cubic Fe_3O_4, which can be readily indexed according to JCPDS file no. 75-0033, and the diffraction peak at $2\theta = 26°$, which can be indexed to (002) reflection of the c-MWCNTs. No obvious peaks from other phases are observed, indicating that the product obtained was a mixture of two phases: cubic Fe_3O_4 and c-MWCNTs. The main peaks of Fe_3O_4 in the XRD pattern are broadened, indicating that the crystalline portion of the Fe_3O_4 particle is very small.

Figure 4 shows the surface groups on c-MWCNTs, MNPs, and MMWCNTs analyzed by FT-IR. Several significant bands in Fig. 4A are attributed to carboxylic acid groups introduced by acid oxidizing (Chen et al. 2011), including the appearance of C=O stretching band at 1,735 cm^{-1}, COO^- asymmetric stretching band at 1,620 cm^{-1}, and O–H stretching band at 3,421 cm^{-1}. While the Fe–O characteristic

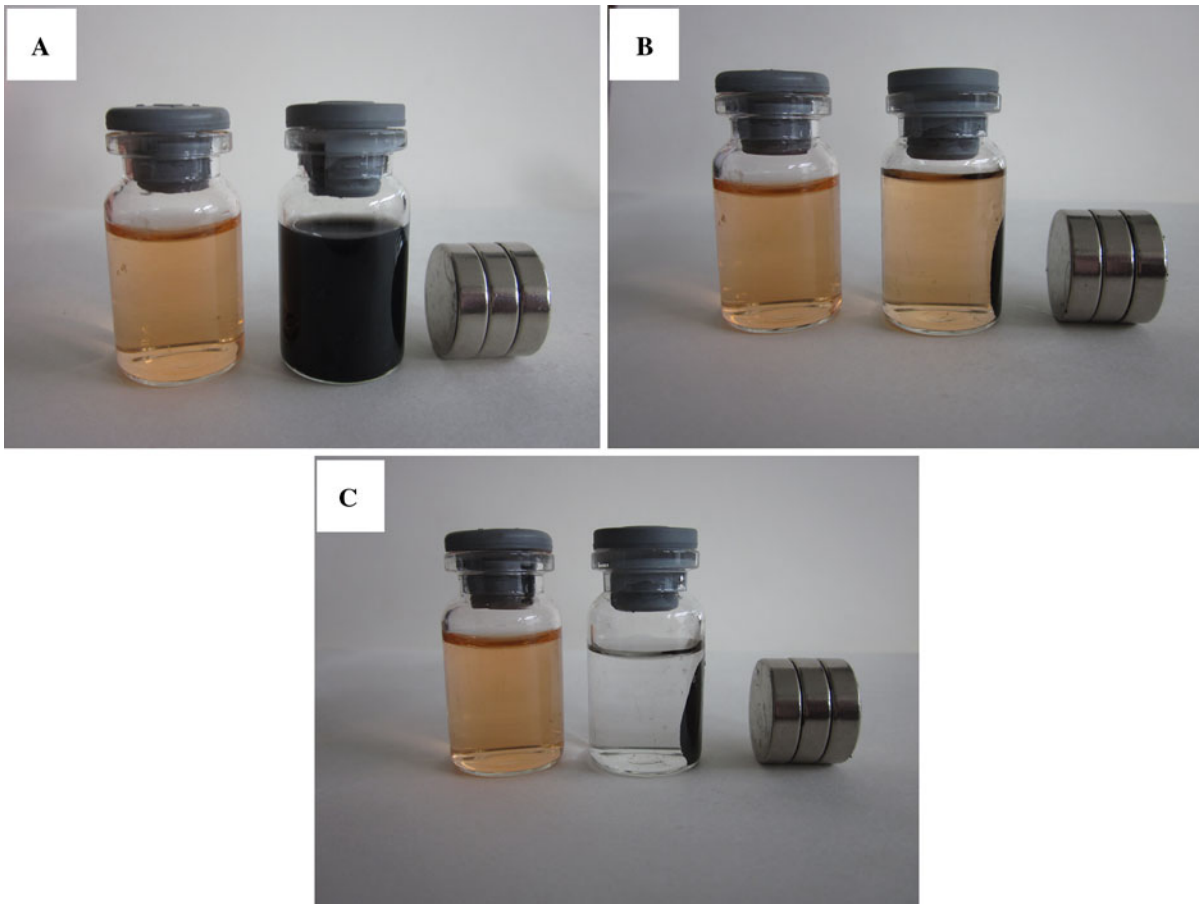

Fig. 2 Photographs of adsorption behavior and magnetic separation: **a** EPI aqueous solution and EPI and c-MWCNTs suspension, **b** EPI aqueous solution and EPI and MNPs suspension, and **c** EPI and EPI and MMWCNTs suspension

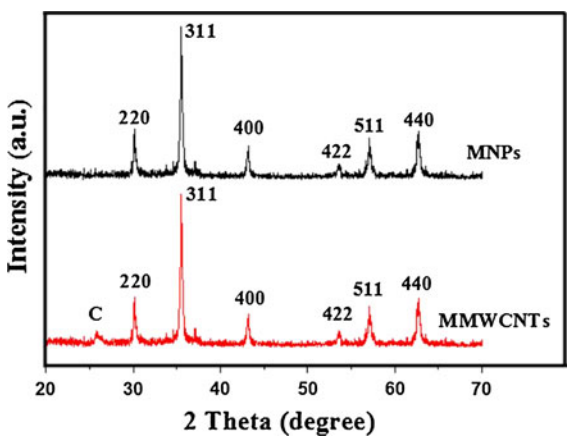

Fig. 3 XRD pattern of MNPs and MMWCNTs

band at 583 cm^{-1} is indicative of Fe_3O_4 (Lu et al. 2010) in Fig. 4B. The FT-IR spectra of MMWCNTs composites (Fig. 4C) appears at 1,735 cm^{-1} for C=O stretching band, 1,620 cm^{-1} for COO^- asymmetric stretching band, 3,421 cm^{-1} for O–H stretching band, and 583 cm^{-1} for Fe–O characteristic band, indicating that MMWCNTs is composed of c-MWCNTs and MNPs.

Kinetics analysis

The adsorption kinetics data of EPI adsorbed on three types of materials are presented in Fig. 5. A rather fast uptake of EPI occurred during the first hour of the adsorption process and a slower stage was followed until the amount of adsorbed EPI reached its equilibrium value. It was also observed that the equilibrium time for c-MWCNTs, MNPs, and MMWCNTs was about 30, 60, and 60 min, respectively.

In our study, two different models were used to investigate kinetic parameters and interpret the

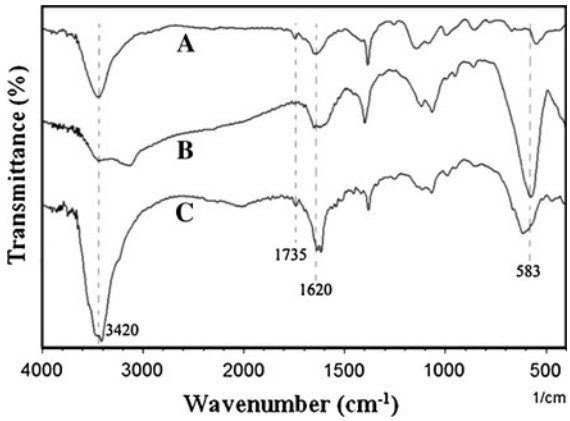

Fig. 4 FT-IR spectrum of c-MWCNTs (*A*), MNPs (*B*), and MMWCNTs (*C*)

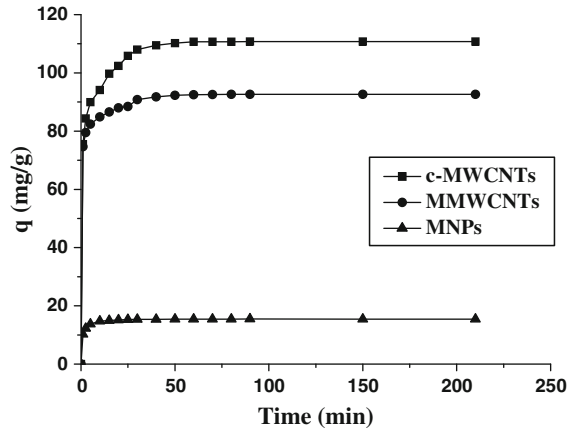

Fig. 5 Kinetic curves for EPI adsorption on different materials (EPI concentration 300 μg/mL, adsorbent dose 0.001 g/mL, temperature 25 °C, pH 7.0)

adsorption kinetic process. The pseudo-first-order model is defined as:

$$q_e - q_t = \lg q_e - \frac{k_1}{2.303} t \quad (1)$$

where k_1 is the equilibrium rate constant for pseudo-first-order; q_e and q_t (mg/g) respectively represent the amounts of EPI adsorbed at equilibrium and time t (min). We should obtain a straight line from a plot of $(q_e - q_t)$ versus t, however, the result does not follow the pseudo-first-order model.

The pseudo-second-order model is described as follows:

$$\frac{t}{q_t} = \frac{t}{q_e} + \frac{1}{k_2 q_e^2} \quad (2)$$

where q_e and q_t (mg/g) respectively represent the amounts of EPI adsorbed at equilibrium and time t (min), and k_2 is the rate constant. The q_e and k_2 values can be calculated from the slope and intercept of the linear plot of t/q_t versus t. A linear relationship between t/q_t and t with high correlation coefficients shows that the pseudo-second-order model is more applicable than the pseudo-first-order model.

Table 1 lists the results of adsorption kinetics using the fittings of pseudo-second-order model. This result demonstrates that the adsorption rate of EPI depends on the concentration of EPI at the adsorbent surface and the absorbance of these absorbed at equilibrium (Sun and Wang 2006).

Adsorption isotherms

The adsorption isotherm expresses the relationship between equilibrium adsorption capacity and equilibrium concentration at constant temperature. The adsorption isotherms of EPI on c-MWCNTs, MNPs, and MMWCNTs at 25 °C are shown in Fig. 6. In general, the equilibrium adsorption capacity increases with the increment of equilibrium concentration, but the increase of equilibrium adsorption capacity is stopped when the initial concentration has reached a certain value.

The Langmuir model and the Freundlich model are employed to study the adsorption isotherm. The Langmuir model is applicable for monolayer adsorption on a surface with limited identical sites and the equation is expressed as:

Table 1 Adsorption kinetic constants for EPI adsorption on c-MWCNTs, MMWCNTs, and MNPs at 25 °C

Materials	Pseudo-first-order kinetic model				Pseudo-second-order kinetic model		
	$q_{e,\exp}$ (mg/g)	$q_{e,\mathrm{cal}}$ (mg/g)	k_1 (min)	R_1^2	$q_{e,\mathrm{cal}}$ (mg/g)	k_2 (g/mg/min)	R_2^2
MNPs	15.36	4.49	0.3807	0.9762	15.67	0.0988	0.9999
c-MWCNTs	110.69	37.39	0.1985	0.9931	112.36	1.9226	0.9994
MMWCNTs	92.54	19.73	0.1927	0.9661	93.46	0.0131	0.9997

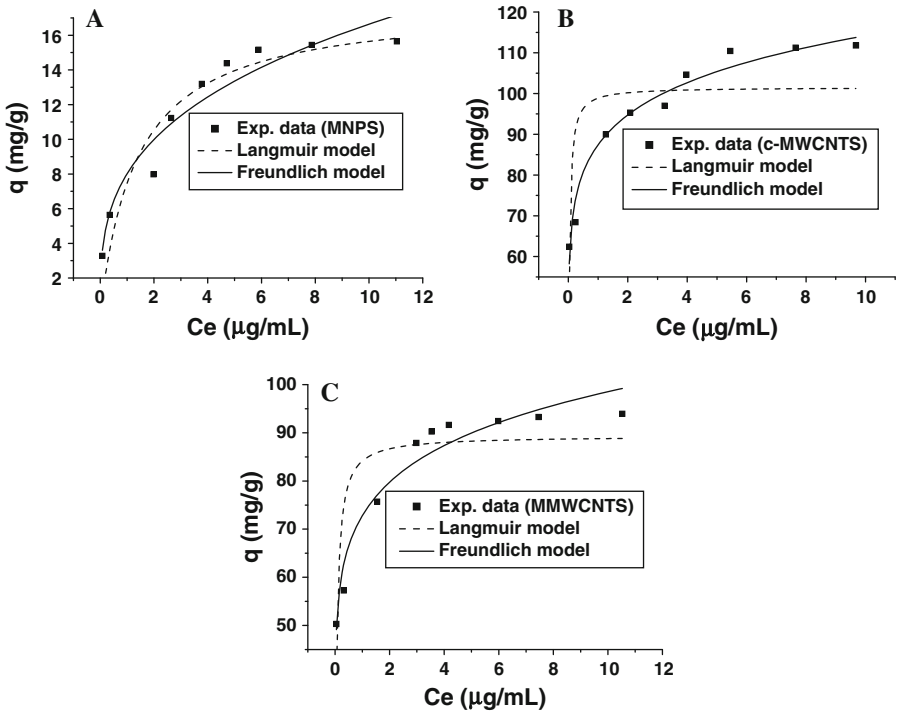

Fig. 6 Adsorption isotherm of EPI on different materials (adsorbent dose 0.001 g/mL, temperature 25 °C, pH 7.0, equilibrium time 4 h)

$$\frac{1}{q_e} = \frac{1}{Q_{\mathrm{m}}} + \frac{1}{Q_{\mathrm{m}} C_e K_L}. \tag{3}$$

where q_e is the adsorbed EPI concentration at equilibrium (mg/g); C_e is the remaining EPI concentration in solution at equilibrium (mg/L); Q_{m} is the maximum adsorption capacity; and K_L, the Langmuir constant, is pertinent to affinity of the binding sites.

The Freundlich isotherm describes the adsorption on a heterogeneous surface with the exponential distribution of sites and their energies. This isotherm equation is expressed as:

$$\lg q_e = \lg K_F + \frac{\lg C_e}{n} \tag{4}$$

where q_e is the adsorbed EPI concentration at equilibrium (mg/g); C_e represents remaining EPI concentration in solution at equilibrium (mg/L); K_F and n are the Freundlich constants, which respectively represent the adsorption capacity and the adsorption strength.

The equilibrium adsorption data of EPI on c-MWCNTs, MMWCNTs, and MNPs were analyzed by Langmuir and Freundlich models (Fig. 6). The correlation coefficient R^2 values and the constants obtained from the two models are summarized in Table 2. The results showed that the correlation coefficients of Freundlich exceeded 0.93, indicating that the Freundlich model gave better fit than the Langmuir model on the adsorption of EPI. According to K_F, the order of adsorption capacity was as follows: c-MWCNTs > MMWCNTs > MNPs. These data also demonstrated that the values of the Freundlich exponent n of c-MWCNTs, and MMWCNTs were greater than those of MNPs, confirming that the adsorption process is successful and the two materials—c-MWCNTs and MMWCNTs are excellent adsorbents for anticancer drug EPI.

Table 2 Freundlich and Langmuir isotherm model constants and correlation coefficients for EPI adsorption on different materials at 25 °C

Materials	Freundlich isotherm model			Langmuir isotherm model		
	K_F	n	R^2	Q_{m}	K_L	R^2
MNPs	8.02	3.15	0.9318	17.80	0.73	0.8863
c-MWCNTs	87.43	8.62	0.9640	101.53	37.12	0.5538
MMWCNTs	72.82	7.62	0.9432	89.35	16.17	0.6895

Influence of pH and temperature

The pH has a significant impact on the adsorption process. According to hydrophobic anthracycline and hydrophilic sugar moiety of EPI, it is known as an amphiphilic weak base ($pK_a = 7.7$). In our study, we investigated the effect of pH on the adsorption capacity of EPI on MMWCNTs. The range of pH we investigated on EPI adsorption tests was between 5.7 and 8.0. The results showed that the loading capacity of EPI on MMWCNTs increased from 89.12 to 96.15 mg/g as pH was increased from 5.7 to 8.0. This indicates that the amount of EPI loaded on MMWCNTs is pH-dependent. There are three possible interactions between EPI and MMWCNTs which are known as followed: (a) π–π stacking interaction; (b) hydrophobic interaction; and (c) hydrogen-bonding interaction between the EPI –OH and the nanotubes surface –COOH group. The apparent pH effect of EPI adsorption onto MMWCNTs depends on the counteraction between the decrease of hydrogen bonding interaction and the increase of both π–π stacking interaction and hydrophobic interaction. The results showed that the adsorption capacity was enhanced with the increment of pH. This indicates that the decrease of the hydrogen-bonding effect is not too strong to balance the increase of both π–π stacking interaction and hydrophobic interaction.

The influence of temperature on adsorption capacity of EPI onto MMWCNTs was also investigated over a range of temperature from 20 to 80 °C. It was observed that the amount of EPI adsorbed decreased when temperature increased from 20 to 80 °C. Higher temperature was unfavorable to the adsorption process, indicating that this adsorption is an exothermic process. This result is consistent with the report from Yan et al. (2008). Thus, the room temperature is more appropriate for the preparation of EPI-loaded MMWCNTs.

In vitro release of EPI

To evaluate the release of EPI-loaded MMWCNTs, we have performed release experiments in vitro. The cumulative release ratio (%) is given by the ratio of the amount of EPI desorbed/adsorbed. Figure 7 indicates that the adsorption of EPI on MMWCNTs was reversible and the cumulative release ratio had increased with time. All of the release curves show a rapid release process in the initial stage, followed by a slow and sustained release process, which seems to continue for a prolonged period of time. Moreover, the

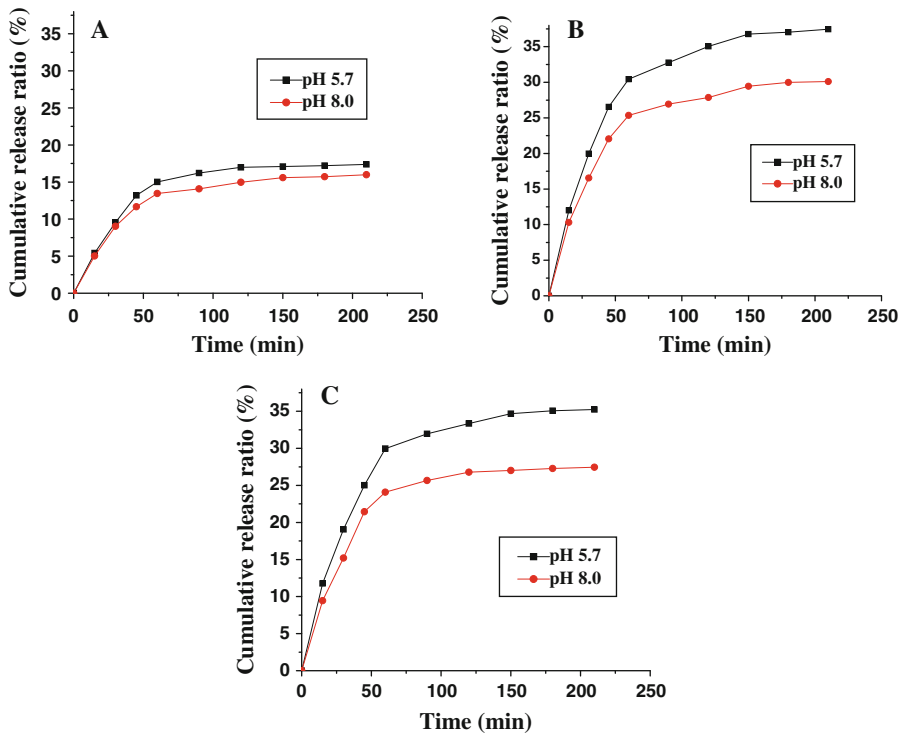

Fig. 7 EPI release from MNPs (**a**), c-MWCNTs (**b**), and MMWCNTs (**c**) in PBS buffer at 37 °C

Table 3 Release of EPI from different materials at different pH

Materials	Release percentage (%) ($n = 6$)			
	pH 5.7	pH 6	pH 7	pH 8
MNPs	17.39	16.94	16.57	15.98
c-MWCNTs	37.45	35.98	32.56	30.11
MMWCNTs	35.23	33.92	30.22	27.46

amount of EPI released from MMWCNTs, shaken for 3.5 h, in the acidic solution was larger than that in the neutral solution (Table 3). This phenomenon can be mainly attributed to the decrease of both π–π stacking interaction and hydrophobic interaction at low pH. It has been reported that the local pH of solid tumor (pH < 6.5) was lower than that of normal tissue (pH 7.4) (Zhang et al. 2009). Therefore, the pH-sensitive release behavior of EPI from MMWCNTs may benefit the tumor treatment.

Mechanism research

Figure 8 illustrates the proposed overall synthetic procedure of MMWCNTs and its adsorption with EPI. Treating MWCNTs with concentrated H_2SO_4/HNO_3 mixture is a classic method of creating a large amount of negatively charged functional groups such as carboxyl on the surface of MWCNTs. Positive metal ions in the system and the carboxylic groups would interact through electrostatic attraction, and the positive metal ions can be served as nucleation precursors. In our study, ferric ions in this system are likely attached to some particular positions of c-MWCNTs. In this solvothermal process, the reduction reaction can turn some of these ferric ions into ferrous ions and then they can coprecipitate into Fe_3O_4 crystallites. According to the aggregation of Fe_3O_4 nanocrystallites, some researchers supposed that the aggregation growth will be intrigued when the driving force from Brownian motion and van der Waals attraction surpasses the repulsive force (Banfield et al. 2000). Currently, the decrease of the high surface energy is the main motive power for the oriented aggregation of nanocrystals. Also, in our case, dipolar interactions between the magnetic nanocrystals are related to their oriented aggregation. Moreover, the greater viscosity of non-aqueous phase in our system could slow down the aggregating rate of Fe_3O_4 nanocrystals. When provided with sufficient time, Fe_3O_4 nanocrystals can rotate at the low-energy configuration interface (He et al. 2004) which is helpful to the oriented aggregation.

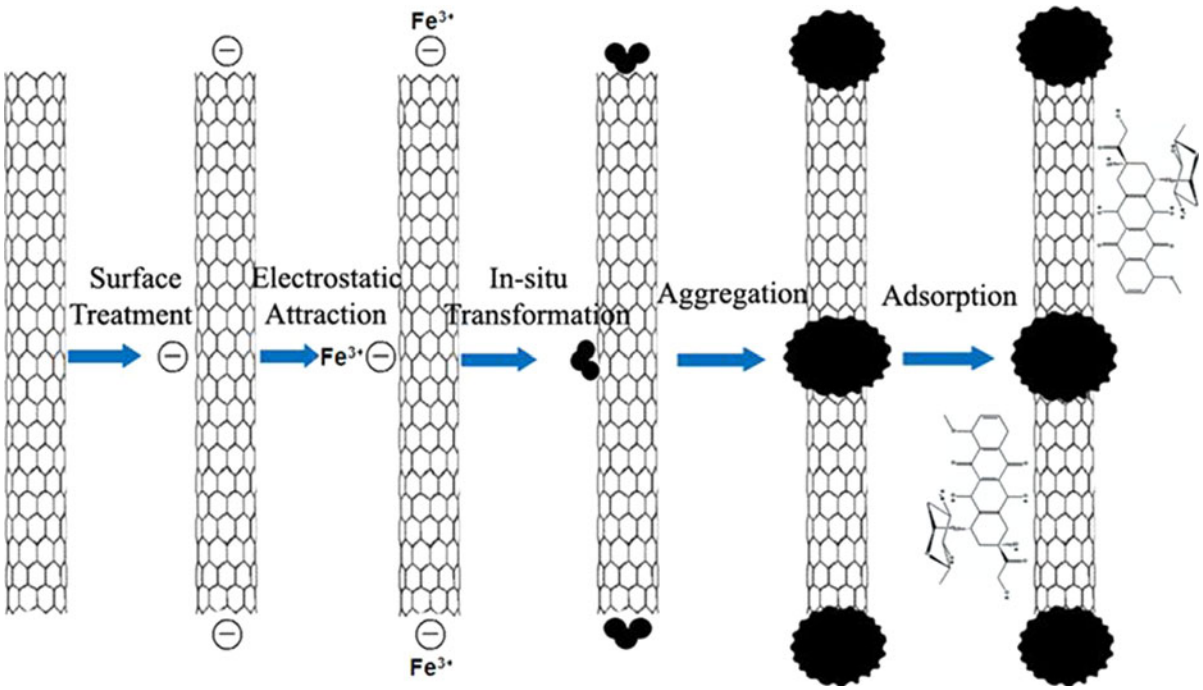

Fig. 8 Schematic illustration of Fe_3O_4 beads on MWCNTs in the solvothermal system

Control experiments indicated that the location, size, and denseness of Fe_3O_4 beads along MWCNTs as well as the structure of Fe_3O_4/MWCNTs composite can be altered by changing the experimental parameters such as duration of both acid treatment and solvothermal treatment, amount of ferric precursor used, and EG/DEG ratio (v/v).

The duration of MWCNTs acid treatment with a concentrated H_2SO_4/HNO_3 mixture has a great influence on both loading position of Fe_3O_4 onto MWCNTs and structure of Fe_3O_4/MWCNTs composite. The duration of acid treatment for the synthesis of Necklace-like Fe_3O_4/MWCNTs nanostructure with Fe_3O_4 beads on MWCNTs was 6 h (Fig. 9b). When we prolonged the MWCNTs acid treatment to 14 h, interesting net-like magnetite/MWCNTs nanostructures were formed, in which Fe_3O_4 spheres, acting as joint, were connected by shortened MWCNTs (Fig. 9c). Oxidizing acids such as a concentrated H_2SO_4/HNO_3 mixture were used to open the ends of MWCNTs and also to cut it. At the earlier stage of acid treatment, carboxylic groups would be generated both at the ends and along the sidewall of MWCNTs, so it is suggested that when using this kind of c-MWCNTs, the formed Fe_3O_4/MWCNTs nanostructure will be Necklace-like type, whereas with the 14 h treatment time, the pristine MWCNTs have been cut into shorter material. Meanwhile, the Fe_3O_4 particles would be preferentially attached on the tips of shortened MWCNTs, where the density of carboxylic groups is supposed to be the highest. As a result, these short MWCNTs connect Fe_3O_4 spheres together and form novel net-like structure (Jia et al. 2007).

As shown form Eq. 5–8, $FeCl_3$, NaOAc, Na acrylate, EG, and DEG play important roles in the formation of MMWCNTs. It has been reported that Fe^{3+} cannot be reduced by EG alone (Cao et al. 2008). NaOAc was destined to assist the EG/DEG in reducing $FeCl_3$ into Fe_3O_4 by modifying the alkalinity of the system. The hydrolysis rate of $FeCl_3$ could be accelerated by increasing alkalinity to promote the formation of larger Fe_3O_4 nanocrystals (Shen et al.

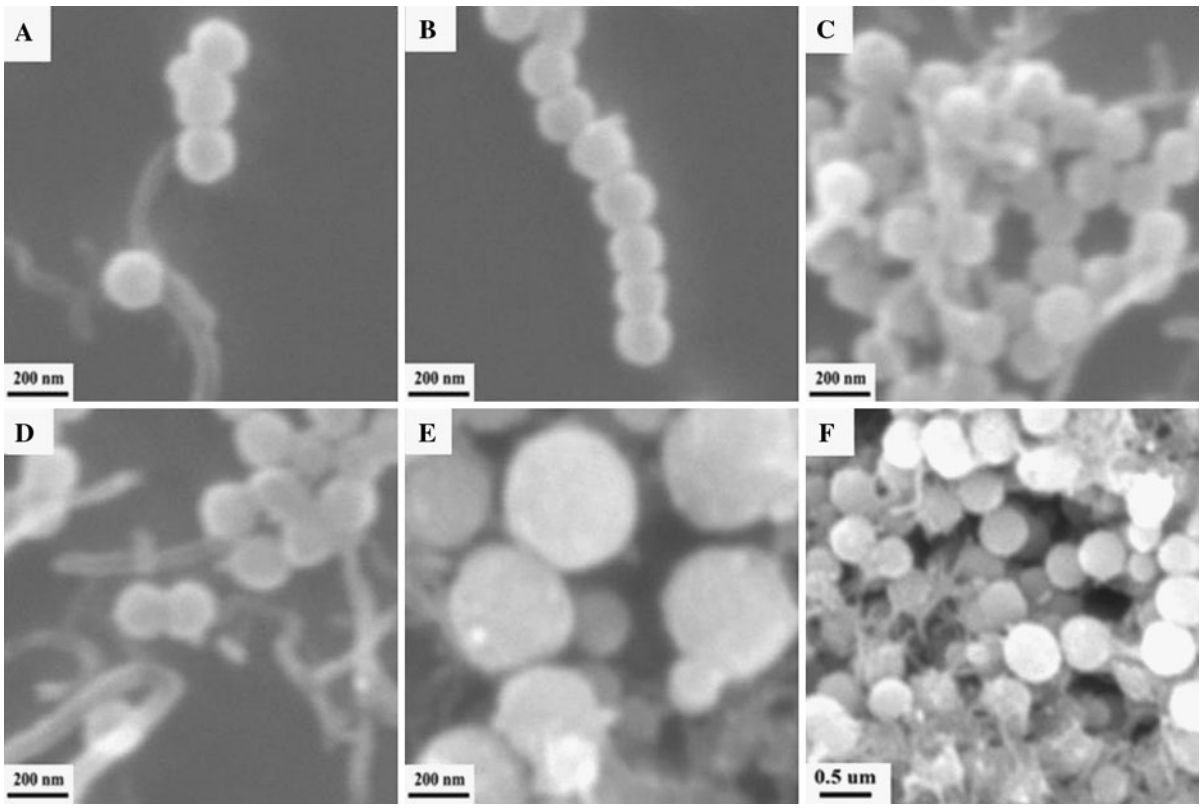

Fig. 9 Influence of starting Fe^{3+} concentration and time in acid treatment of MWCNTs: **a** 4.5 mmol, 6 h; **b** 9 mmol, 6 h; **c** 9 mmol, 14 h; and influence of EG/DEG ratio during solvothermal process: **d** 5/15; **e** 10/10; **f** 15/5

2012). Sodium acrylate was coated with the formed Fe_3O_4 nanograins due to the strong coordination between ferric ions and carboxylate. The formed polyacrylate in situ would stabilize the primary Fe_3O_4 nanograins, and confine them to form larger Fe_3O_4 grains in the recrystallization process (Lin et al. 2005). EG plays both roles as a reducing agent and as a solvent during the formation of the Fe_3O_4 particles (Xuan et al. 2009). Since the reaction temperature in the sealed container was 200 °C, just slightly higher than the boiling point of EG (196 °C), EG may exist as a superfluid. When DEG (boiling point = 240 °C) was introduced together with EG in the reaction system, quite surprisingly, the size of the Fe_3O_4 particles can be successfully reduced by only changing the EG/DEG ratio. Under the same experimental condition, the size of the Fe_3O_4 particles significantly increased with a decreasing amount of DEG. The diameters of the as-prepared Fe_3O_4 particles were ranging from 100 to 250 and 350 nm when the EG/DEG ratio (v/v) changed from 5/15 to 10/10 and 15/5, respectively (Fig. 9d–f).

$$HO - CH_2 - CH_2 - OH \rightarrow CH_3CHO + H_2O \quad (5)$$

$$CH_3COO^- + H_2O \rightarrow OH^- + CH_3COOH \quad (6)$$

$$2CH_3CHO + 2F_e^{3+} + 2OH^- \rightarrow CH_3COCOCH_3 + 2F_e^{2+} + 2H_2O \quad (7)$$

$$2F_e^{3+} + F_e^{2+} + 8OH^- \rightarrow Fe_3O_4 + 4H_2O \quad (8)$$

Furthermore, by raising the quantity of starting ferric precursor, the denseness of the Fe_3O_4 beads along the MWCNTs increased, while the size of magnetite beads was just slightly greater (Fig. 9a, b). It is rational that the rising of Fe^{3+} concentration would generate more Fe_3O_4 nanocrystallites and increase the denseness of Fe_3O_4 beads along MWCNTs. The investigation into the effect of the reaction duration of the solvothermal process indicated that the size of Fe_3O_4 beads did not grow as the reaction time increased from 8 to 10 and 12 h, because the Fe_3O_4 particle formation is a very rapid process (Xuan et al. 2009).

At last, we have found that EPI could strongly and rapidly be adsorbed on MMWNT. By investigating the factors which influence adsorption behavior, we observed that the driving force is attributed to π–π stacking interaction between EPI and MWCNTs graphene surface. This result is consistent with those of our recent publication (Chen et al. 2011).

Conclusion

In summary, a simple, effective, and reproducible solvothermal method was developed to synthesize a series of MMWCNTs nanostructures. In this study, the time used for acid treatment of MWCNTs with a H_2SO_4/HNO_3 mixture is an important factor for the loading of Fe_3O_4 into MWCNTs and for the formation of Fe_3O_4/MWCNTs composite. When prolonging the MWCNTs acid-treatment time from MMWCNTs nanostructures changed from necklace-like to net-like structures, in which Fe_3O_4 spheres were connected to the shortened MWCNTs. In the same time, the Fe_3O_4 particle size was found to be successfully reduced by varying the EG/DEG ratio only. Thus, our results clearly demonstrated the high flexibility of this synthesis method.

Concerning the adsorption behavior of anticancer drug EPI on MMWCNTs, we found that EPI is strongly and rapidly adsorbed on WMWCNTs by π–π stacking interaction between EPI and MMWCNTs graphene surface. The kinetic data are well suitable for a pseudo-second-order model. The adsorption process follows the Freundlich model and it is exothermic.

Finally, this work provides a new insight for the MMWCNTs synthesis and can improve the knowledge about the properties and relationships between MMWCNTs and EPI. Our technique described here for the adsorption of anticancer drug EPI on MMWCNTs provides excellent results and could be extended to the adsorption of other drugs on CNTs constructed with Fe_3O_4 spheres or other inorganic compounds, such as ferrite and metal oxide. Additionally, our novel MMWCNTs endowed with high magnetic properties, large adsorption surfaces, and excellent adsorption capacities is an ideal vehicle for loading EPI or other drugs. These findings might help us to develop new theories and applications for the magnetic targeted drug delivery system in order to enhance drug efficacy and to diminish its toxicity in humans.

Acknowledgments This study was supported by Graduate Students Innovative Projects of Jiangsu Province (No. CXZZ11_0812), Zhejiang Provincial Natural Science Foundation of China (Grant No. Y4110235) and the Fundamental Research Funds for the Central Universities (Program No. JKY2011008). The authors are delighted to acknowledge discussions with colleagues in their research group.

References

Banfield JF, Welch SA, Zhang H, Ebert TT, Penn RL (2000) Aggregation-based crystal growth and microstructure development in natural iron oxyhydroxide biomineralization products. Science 289:751–754

Bianco A, Kostarelos K, Prato M (2005) Applications of carbon nanotubes in drug delivery. Curr Opin Chem Biol 9:674–679

Bottini M, Magrini A, Rosato N, Bergamaschi A, Mustelin T (2006) Dispersion of pristine single-walled carbon nanotubes in water by a thiolated organosilane: application in supramolecular nanoassemblies. J Phys Chem B 110:13685–13688

Cai KY, Luo Z, Hu Y, Chen XY, Liao YJ, Yang L, Deng LH (2009) Magnetically triggered reversible controlled drug delivery from microfabricated polymeric multireservoir devices. Adv Mater 21:4045–4049

Cao S-W, Zhu Y-J, Chang J (2008) Fe_3O_4 polyhedral nanoparticles with a high magnetization synthesized in mixed solvent ethylene glycol–water system. New J Chem 32:1526–1530

Chen Z, Pierre D, He H, Tan S, Pham-Huy C, Hong H, Huang J (2011) Adsorption behavior of epirubicin hydrochloride on carboxylated carbon nanotubes. Int J Pharm 405:153–161

Correa-Duarte MA, Grzelczak M, Salgueiriño-Maceira V, Giersig M, Liz-Marzán LM, Farle M, Sierazdki K, Diaz R (2005) Alignment of carbon nanotubes under low magnetic fields through attachment of magnetic nanoparticles. J Phys Chem B 109:19060–19063

Dumortier H, Lacotte S, Pastorin G, Marega R, Wu W, Bonifazi D, Briand J-P, Prato M, Muller S, Bianco A (2006) Functionalized carbon nanotubes are non-cytotoxic and preserve the functionality of primary immune cells. Nano Lett 6:1522–1528

Gai QQ, Qu F, Liu ZJ, Dai RJ, Zhang YK (2010) Superparamagnetic lysozyme surface-imprinted polymer prepared by atom transfer radical polymerization and its application for protein separation. J Chromatogr A 1217:5035–5042

Gao C, Li W, Morimoto H, Nagaoka Y, Maekawa T (2006) Magnetic carbon nanotubes: synthesis by electrostatic self-assembly approach and application in biomanipulations. J Phys Chem B 110:7213–7220

Gao L, Zhuang J, Nie L, Zhang J, Zhang Y, Gu N, Wang T, Feng J, Yang D, Perrett S, Yan X (2007) Intrinsic peroxidase-like activity of ferromagnetic nanoparticles. Nat Nano 2:577–583

Georgakilas V, Tzitzios V, Gournis D, Petridis D (2005) Attachment of magnetic nanoparticles on carbon nanotubes and their soluble derivatives. Chem Mater 17:1613–1617

Graff RA, Swanson TM, Strano MS (2008) Synthesis of nickel–nitrilotriacetic acid coupled single-walled carbon nanotubes for directed self-assembly with polyhistidine-tagged proteins. Chem Mater 20:1824–1829

He T, Chen D, Jiao X (2004) Controlled synthesis of Co_3O_4 nanoparticles through oriented aggregation. Chem Mater 16:737–743

Hong C-Y, You Y-Z, Pan C-Y (2005) Synthesis of water-soluble multiwalled carbon nanotubes with grafted temperature-responsive shells by surface RAFT polymerization. Chem Mater 17:2247–2254

Jia B, Gao L, Sun J (2007) Self-assembly of magnetite beads along multiwalled carbon nanotubes via a simple hydrothermal process. Carbon 45:1476–1481

Kim Y, Cho J, Ansari S, Kim H, Dar M, Seo H, Kim G, Lee D, Khang G, Shin H (2006) Immobilization of avidin on the functionalized carbon nanotubes. Synth Met 156:938–943

Kim IT, Nunnery GA, Jacob K, Schwartz J, Liu X, Tannenbaum R (2010) Synthesis, characterization, and alignment of magnetic carbon nanotubes tethered with maghemite nanoparticles. J Phys Chem C 114:6944–6951

Korobeinyk AV, Whitby RLD, Niu JJ, Gogotsi Y, Mikhalovsky SV (2011) Rapid assembly of carbon nanotube-based magnetic composites. Mater Chem Phys 128:514–518

Lijima S (1991) Helical microtubules of graphitic carbon. Nature 354:56–58

Lin C-L, Lee C-F, Chiu W-Y (2005) Preparation and properties of poly(acrylic acid) oligomer stabilized superparamagnetic ferrofluid. J Colloid Interface Sci 291:411–420

Liu Z, Sun X, Nakayama-Ratchford N, Dai H (2007) Supramolecular chemistry on water-soluble carbon nanotubes for drug loading and delivery. ACS Nano 1:50–56

Lu W, Shen Y, Xie A, Zhang W (2010) Green synthesis and characterization of superparamagnetic Fe_3O_4 nanoparticles. J Magn Magn Mater 322:1828–1833

Nam J-M, Thaxton CS, Mirkin CA (2003) Nanoparticle-based bio-bar codes for the ultrasensitive detection of proteins. Science 301:1884–1886

Pantarotto D, Singh R, McCarthy D, Erhardt M, Briand JP, Prato M, Kostarelos K, Bianco A (2004) Angew Chem Int Ed 43:5242

Pavani R, Vinay K (2011) Carbon nanotubes and pharmaceutical applications. Int Res J Pharm 2:15–21

Shen W, Chen X, Shi Y, Shi M, Chen H (2012) Synthesis of monodisperse and single-crystal Fe_3O_4 hollow spheres by a solvothermal approach. Mater Chem Phys 132:987–992

Sun S, Wang A (2006) Adsorption kinetics of Cu(II) ions using *N*,*O*-carboxymethyl-chitosan. J Hazard Mater 131:103–111

Sun S, Murray CB, Weller D, Folks L, Moser A (2000) Monodisperse FePt nanoparticles and ferromagnetic FePt nanocrystal superlattices. Science 287:1989–1992

Wang HF, Wang J, Deng XY, Sun HF, Shi ZJ, Gu ZN, Liu YF, Zhao YL (2004) J Nanosci Nanotechnol 4:1019

Xuan S, Wang Y-XJ, Yu JC, Cham-Fai LK (2009) Tuning the grain size and particle size of superparamagnetic Fe_3O_4 microparticles. Chem Mater 21:5079–5087

Yan XM, Shi BY, Lu JJ, Feng CH, Wang DS, Tang HX (2008) Adsorption and desorption of atrazine on carbon nanotubes. J Colloid Interface Sci 321:30–38

Yang D, Yang F, Hu J, Long J, Wang C, Fu D, Ni Q (2009) Hydrophilic multi-walled carbon nanotubes decorated with magnetite nanoparticles as lymphatic targeted drug delivery vehicles. Chem Commun 7(29):4447–4449

Zhang X, Meng L, Lu Q, Fei Z, Dyson PJ (2009) Targeted delivery and controlled release of doxorubicin to cancer cells using modified single wall carbon nanotubes. Biomaterials 30:6041–6047

Zhu HY, Jiang R, Xiao L, Zeng GM (2010) Preparation, characterization, adsorption kinetics and thermodynamics of novel magnetic chitosan enwrapping nanosized γ-Fe_2O_3 and multi-walled carbon nanotubes with enhanced adsorption properties for methyl orange. Bioresour Technol 101:5063–5069